Investigation of the Absorption Properties of Sputtered Tin Sulfide Thin Films for Photovoltaic Applications

R. E. Banai[1], H. Lee[1], M. Lewinsohn[1], M. A. Motyka[1], R. Chandrasekharan[1], N. J. Podraza[2], J. R. S. Brownson[1], and M. W. Horn[1]

[1]The Pennsylvania State University, University Park, PA, 16802 USA

[2]University of Toledo, Toledo, OH, 43606 USA

***Abstract* — Tin sulfide (SnS) is an absorber with promising optoelectronic properties and low environmental constraints of interest for high efficiency solar cells. Sputtered SnS thin films were deposited at target powers 105-155 W and total pressures of 5 to 60 mTorr in argon. X-ray diffraction patterns confirmed a dominant tin monosulfide phase. The absorption coefficient was determined by spectroscopic ellipsometry and unpolarized spectrophotometry measurements. Both methods show that the films have absorption coefficients above the band gap in the range of 10^5-10^6 cm^{-1}.**

***Index Terms* — absorption, ellipsometry, photovoltaic cells, semiconductor materials, sputtering, tin compounds.**

I. Introduction

The search for better materials for solar cell applications is ongoing. While silicon-based solar cells dominate the market, thin film photovoltaics (PV) are increasingly becoming a major share. This increase is due to lower materials and production costs per module compared to silicon modules. [1] Thin film PV has the potential to dominate the market. However, several manufacturability limitations including environmental concerns, availability, and process scale-up constrain the potential of incumbent devices based on CdTe or $Cu(In_{1-x}Ga_x)Se_2$ as the active layer. Therefore, other materials must be investigated that do not have these limitations and have the potential to achieve high device efficiencies (>20%) required for PV to meet grid parity. Tin monosulfide (SnS) is one such material that has the potential to meet these requirements.

SnS is natively p-type with ideal parameters for a solar cell absorber. SnS has a high absorption coefficient (α) of ~10^5 cm^{-1} in the visible and near infrared range [2], a direct band gap around 1.0-1.3 eV [3], and high free carrier concentration around 10^{16} cm^{-3} [4]. Several deposition methods of SnS have been explored including wet-chemical processing and vacuum based depositions, but the maximum efficiency achieved is below 2% [3]. Deposition by sputtering is known to produce high quality films and is easily scalable, but it has not been explored sufficiently. A few studies have investigated sputtered SnS, but none have fully explored the parameter space [5]. Since sulfur is more volatile than tin, low temperature chemical processing techniques, which allow for better stability, have been used to investigate SnS. However, wet chemistry techniques are not favorable for the manufacturing of PV modules.

A theoretical analysis of SnS solar cell performance using AMPS-1D (Analysis of Microelectronic and Photonic Structures-1-Dimensional) evaluated the potential of SnS solar cells. The analysis has shown that SnS|ZnO solar cell has the practical potential to achieve greater than 20% efficiency in the configuration shown in Fig. 1. Note that it is a 2-dimensional schematic of the 1-D device modeled in AMPS-1D. It is expected that platinum or other high work function metal be implemented as finger front contacts as it is done for silicon cells. Since the model is 1-D and fingers are 3-D structures, the front contact is modeled as a layer with full transparency.

The predicted band diagram from this device configuration showed that using platinum as the front contact and ZnO in the back would cause favorable band bending for the best charge carrier separation. In this configuration, no light can be

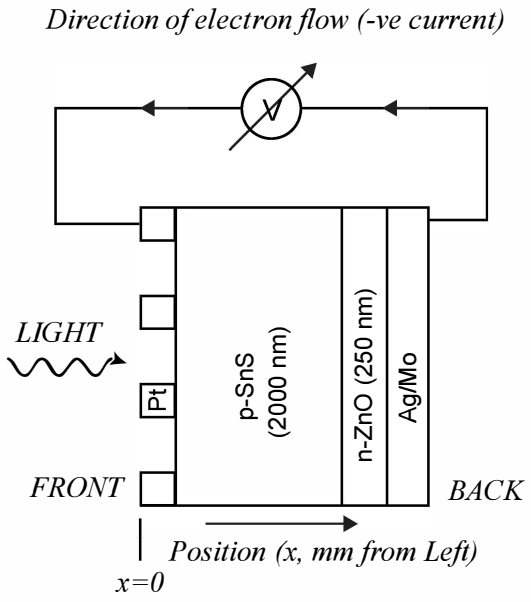

Fig. 1. Schematic of SnS|ZnO solar cell in the substrate configuration. Schematic is for a 1-D model used to predict the efficiency of a SnS|ZnO heterojunction solar cell, with light impinging from the left.

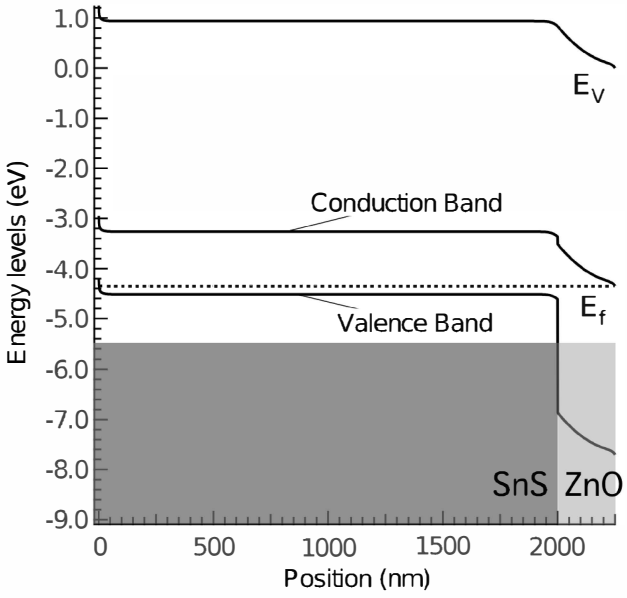

Fig. 2. Predicted Energy Band Diagram for the SnS/ZnO materials system from AMPS-1D modeling program. In this setup, light would enter from the left side. Electron flow is to the right. E_V is the vacuum level and E_f is the Fermi level.

parasitically absorbed in the n-type layer. The band diagram as produced by AMPS-1D is shown in Fig. 2.

In the past, the development of materials for solar cell applications has not had the benefit of theoretical analysis to guide the materials development. Tools such as AMPS-1D are helpful in making theoretical analyses of materials systems prior to experimental investigation. Since SnS has not been investigated in depth for solar cell applications, theoretical analysis will be useful in guiding the early development of the materials system and device structures.

The work completed here begins to investigate the material and optical properties of sputtered SnS films. Previous work in the literature has investigated several deposition methods of SnS such as electrochemical deposition [6] - [7], sulfurization of tin thin films [8], thermal evaporation [9] - [10], and sputtering [5]. Sputtering provides the ability to push the parameter space and has high opportunity to produce reasonable electronic quality PV absorber materials. Sputtering is also proven to be a scalable deposition method for materials over large areas.

The band gap and α of SnS has been measured for various deposition methods. Determining α has not been consistent, which reduces the ability to compare these values. Other analyses found in the literature on SnS have used several methods of determining α via first order approximations [5] - [10]. The analysis presented here will elucidate why SnS is difficult to characterize optically, and why first order approximations do not necessarily produce accurate representations of α.

II. Methods and Materials

A. Sputter Conditions

SnS thin films were deposited in an RF magnetron sputtering system in a downward vertical geometry at room temperature. Target to substrate distance was 17 cm. High vacuum was achieved using a turbomolecular pump. Argon plasmas were produced at 30 mTorr and above, with depositions conducted at pressures ranging from 5 to 60 mTorr. Plasma power ranged from 105 to 155 W. The reflected power for these depositions was within 2% of the applied power. The 3" diameter target used for these depositions was composed of tin monosulfide, of 99.999% purity (LTS Research Laboratories, Inc.). Films were co-deposited on silicon nitride coated silicon wafers and glass microscope slides. Deposition time was adjusted to control film thickness. Colloidal graphite was painted in strips on substrates prior to deposition to infer film thickness. Graphite was removed in an ultrasonic bath with isopropanol for profilometry measurements.

B. Materials Characterization Methods

Several materials characterizations were conducted on the sputter-deposited SnS films. Film thickness was determined using the Tencor P-1 Long Scan Profiler.

Glancing incidence x-ray diffraction (GIXRD) patterns were measured for samples deposited on the microscope slides to determine the crystal structure. The x-ray diffraction patterns were produced using the PANalytical X'Pert Pro MPD. GIXRD measurements were taken at a glancing incident angle of 1° and detected from 5° to 70°. The x-ray patterns of the various tin sulfides have distinct peaks, which were used to determine the phases of the material.

While the films were deposited using a tin monosulfide target, sulfur is known to volatilize easily. It was hypothesized that the films might not deposit in a one-to-one tin-to-sulfur ratio. Electron dispersive spectroscopy (EDS) was used to determine the tin-to-sulfur ratio in these samples. EDS measurements were collected using an EDAX Genesis EDS system on the FEI model XL30 Environmental SEM. EDS data was not compared to a known standard. Current measures are being taken to develop standards for verifying tin-to-sulfur ratios.

Using the ZeissSMT1530, high resolution Field Emission Scanning Electron Microscopy (FESEM) images of the SnS thin films were generated at 3kV and 100kx magnification.

C. Optical Characterization Methods

Two methods were used to determine the absorption characteristics of the thin films. Transmittance and reflectance spectra were measured for SnS-coated glass slides using a Perkin Elmer Lambda 950 spectrophotometer with a maximum spectral range from 300 nm to 2000 nm. The films were highly specular and reflection measurements were calibrated against spectra collected for an aluminum mirror.

If the reflectance (R) is zero, α might be determined by:

$$\alpha = -\frac{1}{d}\ln(T) \qquad (1)$$

where d is the film thickness in centimeters and T is the transmittance. However, as the films have non-negligible reflectance for the range of analysis, Eq. 1 cannot be used to approximate α.

For films with high reflectance in the range of analysis, Eq. 2 must be used to approximate α:

$$\alpha = -\frac{1}{d}\ln\left(\frac{T}{1-R}\right) \qquad (2)$$

where T is transmittance, R is reflectance, and d is the film thickness in centimeters.

SnS films less than 100 nm thick deposited on the silicon nitride-coated crystal silicon substrates were characterized using a multichannel, dual-rotating compensator spectroscopic ellipsometer (model RC2, J.A. Woollam Co.) at 50°, 60°, 70°, and 80° over a spectral range of 0.75 to 5.15 eV. The ellipsometric spectra for these samples were analyzed using a structural model consisting of a semi-infinite crystal silicon substrate / silicon nitride layer / pre-sputtered SnS / bulk SnS film / surface roughness / air ambient structure (CompleteEASE software, J.A. Woollam Co.). The optical properties of the SnS were modeled using Tauc-Lorentz oscillators [11,12]. The optical properties of the surface roughness layer were represented with a Bruggeman effective medium approximation (EMA) consisting of 0.5 bulk layer SnS and 0.5 void fractions. Similarly, the optical properties of the pre-sputtered SnS were represented with a Bruggeman EMA, with the percent of void fraction set as a variable parameter. The unweighted error function between the experimental ellipsometric spectra and the model fit were less than 10^{-2}, with typical values less than 5×10^{-3}, indicating the validity of the optical and structural models. This analysis provided the SnS bulk film thickness, surface roughness thickness, and the complex index of refraction ($N = n + ik$) for SnS.

Using the extinction coefficient (k) determined from spectroscopic ellipsometry data, α was calculated using Eq. 3:

$$\alpha = \frac{4\pi k}{\lambda} \qquad (3)$$

where λ is the wavelength of light in centimeters.

III. Results and Discussion

Characterization of the SnS thin films in this study was two-fold: materials characterization determining the structure and composition of the films, and the optical characterization to determine the absorption.

A. Materials Characterization

To explore the impact of deposition parameters on film growth and microstructure, the impact of target power was studied for films deposited at low and high total pressures. Table I lists the deposition parameters, film thickness, and composition of films characterized in this study. The RF target power had a more significant effect on the deposition rate for films grown at lower pressure as compared to films deposited at high pressure, as shown in Fig. 3. While high deposition rates are positive indicators of the potential for scale-up and manufacturing of this material, it is more crucial to consider the material quality of SnS at this stage of research.

Results of EDS measurements are listed in Table I and indicate that there is a sulfur deficiency in these films. It should be noted that no "standard" SnS has been characterized at present, indicating that there is some uncertainty in the values listed in Table I. The tin-to-sulfur ratio does not vary significantly across all measured samples for a variety of deposition conditions.

X-ray diffraction patterns from the GIXRD measurements showed the primary phase of these SnS films to be tin monosulfide. The pattern data best match PDF#39-354, which

TABLE I
SnS Films Characterized in this Study

Power (W)	Pressure (mTorr)	Thickness (nm)	Sn:S Ratio
105	5	130 ± 20	1:0.75
105	60	250 ± 16	1:0.73
115	10	240 ± 20	--
135	5	224 ± 8	1:0.76
135	60	89 ± 3	1:0.67
145	10	--	--
155	5	300 ± 25	--
155	60	81 ± 3	--

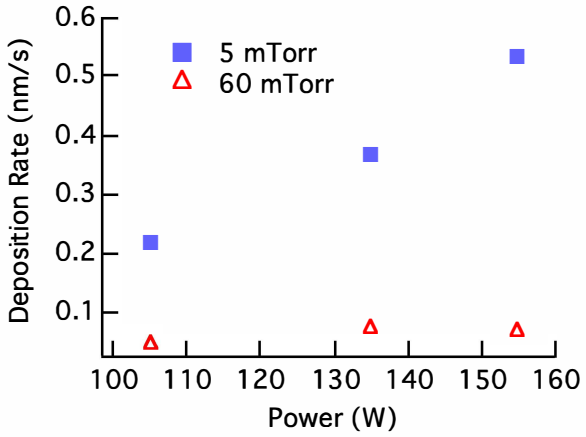

Fig. 3. Deposition rate for SnS films produced at different process powers and pressures.

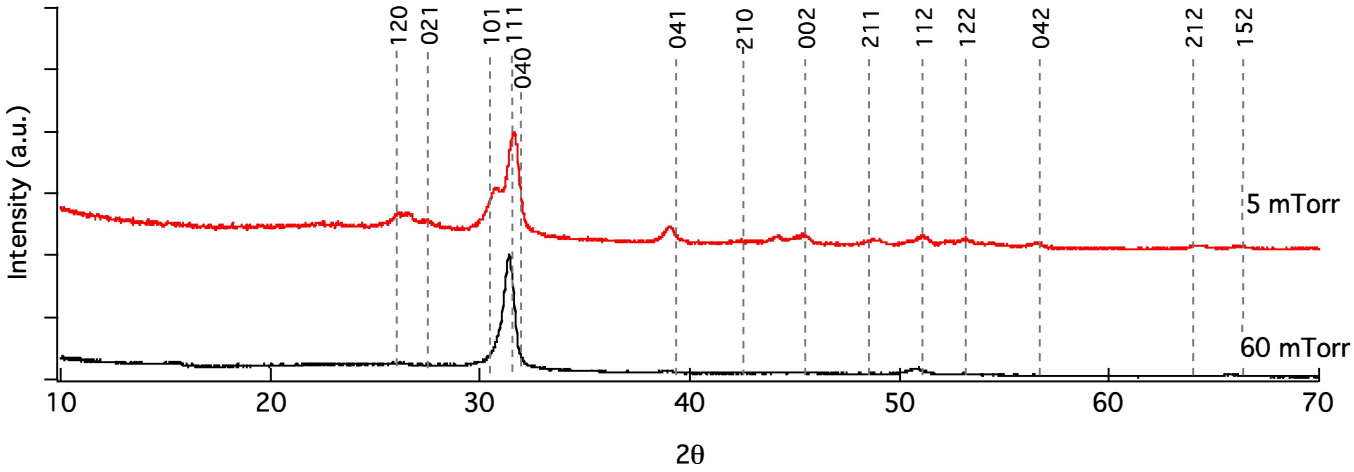

Fig. 4. X-ray diffraction patterns of SnS films deposited at 5 and 60 mTorr total pressure and 105 W target power. Pattern data are matched to PDF# 39-354.

is herzenbergite tin monosulfide (Ortho; *Pbnm; 2/m 2/m 2/m; a=4.3291 b=11.1923 c=3.9838 Z=4*). Fig. 4 shows the XRD patterns of two films deposited at 105 W, with one at 5 mTorr and the second at 60 mTorr. Fig. 5 displays the bond structure and atomic arrangement of herzenbergite. No peaks were identified below 10°, and therefore excluded from the data shown. The films deposited at high pressure have preferential orientation in the <111> direction. Films deposited at low pressure have secondary inclusions of grains with <101> orientation, as well as additional minor peaks of various orientations. It can be noted from Fig. 4 that experimental peaks measured for these films do not exactly match the reference peak positions. This distortion is likely caused by strain in the film and variation of the lattice constant. One study by Nozaki et al. concluded that SnS films can have variable lattice parameters as a result of interfacial interaction between the film and the substrate [13]. For films of comparable thickness to the ones presented here, the lattice distortion continued through the film, perpendicular to the substrate [13]. Similarly, it is likely that interfacial effects between the film and the substrate cause the distortion seen in Fig. 4.

It is likely that the significant difference from stoichiometric SnS to the ratios presented in Table I caused there to be a secondary phase in the films as seen in the GIXRD pattern. Sulfur deficiency is also likely to be the cause for lattice strain and a potential difference in the lattice constant from the standard. Exploration of the measurements will be done in future work including comparisons to known standards.

The data from Figs. 3 and 4 show that the film deposited at 5 mTorr had a high deposition rate but a more random distribution of crystallite orientations compared to the film deposited at 60 mTorr. The sample deposited at 60 mTorr had a slower deposition rate, but primarily one dominant orientation of crystallites. While the herzenbergite SnS matches most of the peaks in these x-ray patterns, the additional peaks suggest that another phase may be present in these films.

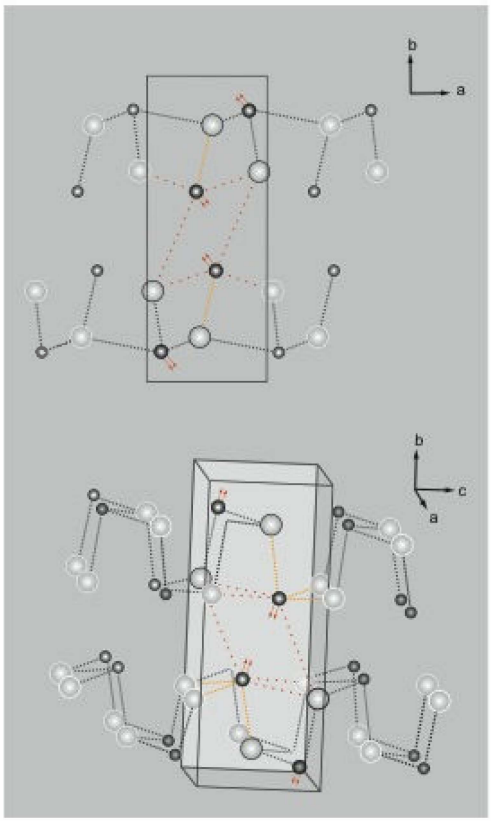

Fig. 5. Structure of SnS. (Top) cross section of the *b*-zone axis (Bottom) 3-D unit cell projection of the *c* zone axis (unit cell tilted). Dark and light spheres represent tin and sulfur atoms, respectively (unit cell: outlined in black). Dashed lines are covalent bonds.

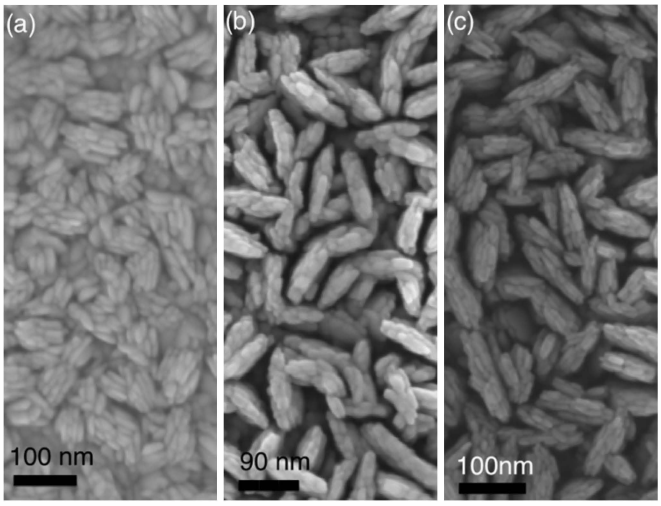

Fig. 6. Field emission scanning electron microscopy images of SnS material deposited at (a) target power 105 W, 5 mTorr total pressure; (b) target power 115 W, 10 mTorr total pressure; and (c) target power 145 W, 10 mTorr total pressure.

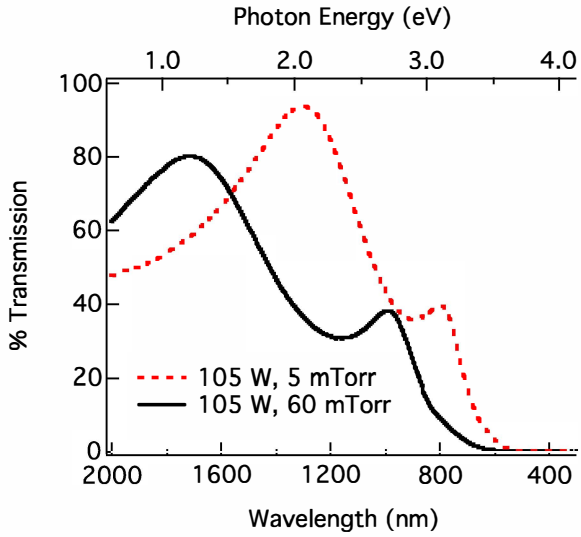

Fig. 7. Transmission spectra for SnS films grown on glass slides.

FESEM imaging of several samples prepared under various deposition conditions shows significant changes in the shape, size, and density of the crystallites. Fig. 6 shows the impact of deposition pressure and power on crystallite formation. The crystallite length in the elongated direction of the material produced at 5 mTorr is shorter than that of the 10 mTorr samples. Additionally, the FESEM image of the film prepared at 5 mTorr indicates that the material is denser than the samples deposited higher pressure. As seen from Fig. 6b and c, RF target power over the 115 to 145 W range does not impact crystallite size, shape, and porosity between grains significantly at 10 mTorr. For an absorber layer in traditional planar photovoltaic devices, it is generally desirable to have large grains and densely packed crystallites with well-passivated grain boundaries. As denser films are produced at higher deposition rates and lower chamber pressures, these films are predicted to yield better performance in photovoltaic devices. However, deposition parameter space must continue to be explored to produce larger grain sized crystallites. The grain size is also expected to increase in size for thicker films.

B. Optical Characterization

Fig. 7 shows the transmittance spectra obtained from spectrophotometry measurements of SnS films on glass slides. Fringes caused by coherent multiple reflections between substrate / film and film / ambient interface are observed for thicker films. The transmittance spectra for thinner films (< 50 nm) do not show interference fringes in the wavelength range shown in Fig. 7. In this case, the frequency of the interference pattern decreases with thickness, although coherent multiple reflections between interfaces still occur. When the unpolarized transmittance and reflectance spectra of the SnS films studied here are analyzed by Eqs. 1 or 2, these interference fringes result in artifacts appearing in spectroscopic α, and thus prevent the accurate determination of α and the band gap. Using unpolarized light, both transmittance and reflectance measurements must be performed on a substrate transparent in the region of the band gap of the film material.

Fig. 8 shows spectroscopic α for a film prepared with a target power of 135 W and a pressure of 60 mTorr and has been extracted from transmittance and reflectance spectra using Eqs. 1 and 2 and by spectroscopic ellipsometry data analysis using Eq. 3. Other thin (< 100 nm) SnS films produced at different sputtering conditions showed behavior trends when analyzed in this manner. As expected, when the reflectance is neglected, significantly different values of α are

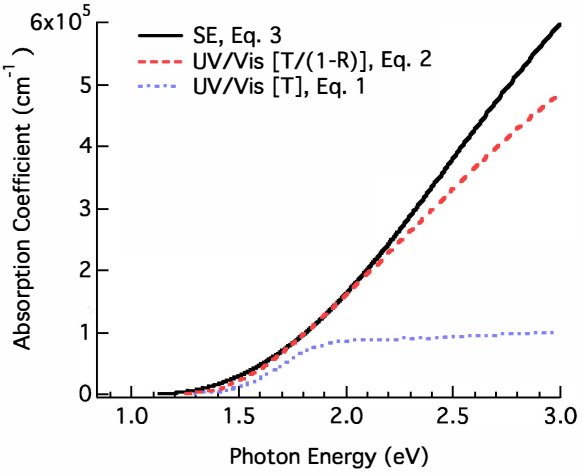

Fig. 8. Absorption coefficient (α), obtained from spectroscopic ellipsometry analysis and ultraviolet-visible spectrophotometry for an SnS film prepared at 135 W target power and 60 mTorr total pressure.

obtained, using Eq. 1 and 2. There is relatively good agreement between α extracted from spectroscopic ellipsometry and the combined analysis of transmittance and reflectance spectra. An absorption onset appears near 1.1-1.2 eV, and continues to increase to values > 10^5 cm^{-1} by 3.0 eV. The high values of α and the absorption onset shown here indicate that SnS matches the solar irradiance spectrum well.

IV. Conclusions and Future Work

Sputtered SnS thin films show promising absorption properties for the absorber layer in future photovoltaic devices. Films were deposited by sputtering and determined to primarily exhibit tin monosulfide phase structure by GIXRD. EDS data has shown that the films have sulfur deficiency which can be attributed to the volatility of sulfur. Future work will utilize calibration by a sample of known stoichiometry to confirm these results. FESEM images show that these thin films have small crystallites, which is generally non-ideal for photovoltaic absorber layers. Sputtering conditions will need to be explored further in order to improve the crystallinity, grain size, and density of the SnS thin films.

Optical characterizations showed the tin sulfide thin films to have α values in the range of 10^5-10^6 cm^{-1}. Both spectrophotometry data and spectroscopic ellipsometry data were used to determine α values of SnS thin films. The discrepancy between the three methods of determining α values result from the nature of the approximations used for the analysis of the spectrophotometry data. Spectroscopic ellipsometry allows for the extraction of both *n* and *k* simultaneous to the determination of layer thicknesses in the sample, but does however lose sensitivity to low values of α near ~10^2-10^3 cm^{-1}. Spectroscopic ellipsometry and unpolarized transmittance spectroscopy measurements combined with a rigorous analysis procedure properly accounting for coherent multiple reflections present for film / substrate sample geometries are expected to yield the most accurate optical properties across the full spectral range. Future work will employ this method of analysis to better characterize SnS films and quantify the band gap.

Acknowledgements

The authors would like to acknowledge several people with their assistance in completing the work presented here. We thank Nichole M. Wonderling (XRD), Beth Jones (XRD), Josh Stapleton (spectrophotometry), and Yao Jin (profilometry) for their assistance with characterizations. Thank you to Lucas Witmer for his assistance with some of the images. Thank you to the Penn State Materials Research Institute and the John & Willie Leone Department of Energy and Mineral Engineering for financial assistance in attending the conference.

References

[1] V.M. Fthenakis, H.C. Kim, and E. Alsema, "Emissions from Photovoltaic Life Cycles," *Environmental Science and Technology*, vol. 42, pp. 2168-2174, 2008.

[2] H. Noguchi, A. Setiyadi, H. Tanamura, T. Nagatomo, and O. Omoto, "Characterization of vacuum-evaporated tin sulfide film for solar cell materials," *Solar Energy Materials and Solar Cells*, vol. 35, pp. 325-331, 1994.

[3] K.T. Ramakrishna Reddy, N. Koteeswara Reddy, and R.W. Miles, "Photovoltaic Properties of SnS based solar cells," *Solar Energy Materials and Solar Cells*, vol. 90, pp. 3041-3046, 2006.

[4] B. Subramanian, C. Sanjeeviraja, and M. Jayachandran, "Cathodic Electrodeposition and Analysis of SnS Films for Photoelectrochemical Cells," *Materials Chemistry and Physics*, vol. 71, pp. 40-46, 2001.

[5] K. Hartman, J.L. Johnson, M.I. Bertoni, D. Recht, M. Aziz, Michael A. Scarpulla, and T. Buonassisi, "SnS thin-films by RF sputtering at room temperature," *Thin Solid Films*, vol. 519, pp. 7421–7424, 2011.

[6] S. Cheng, G. Chen, Y. Chen, and C. Huang, "Preparation and Properties of SnS film grown by two-stage process," *Optical Materials*, vol. 29, pp. 439-444, 2006.

[7] J.R.S. Brownson, C. Georges, and C. Levy-Clement, "Synthesis of a delta-SnS Polymorph by Electrodeposition," *Chemical Materials*, vol. 18, pp. 6397-6402, 2006.

[8] F. Jiang, H. Shen, W. Wang, and L. Zhang, "Preparation of SnS Film by Sulfurization and SnS/a-Si Heterojunction Solar Cells," *Journal of the Electrochemical Society*, vol. 159, pp. H235-H238, 2011.

[9] S.S. Hedge, A.G. Kunjomana, K.A. Chandrasekharan, K. Ramesh, and M. Prashantha, "Optical and electrical properties of SnS semiconductor crystals grown by physical vapor deposition technique," *Physica B*, vol. 406, pp. 1143-1148, 2011.

[10] S.A. Bashkirov, V.F. Gremenok, and V.A. Ivanov, "Physical Properties of SnS Thin Films Fabricated by Hot Wall Deposition," *Semiconductors*, vol. 45, pp. 765-769, 2010.

[11] G.E. Jellsion, Jr. and F.A. Modine, "Parameterization of the optical functions of amorphous materials in the interband region," *Applied Physics Letters*, vol. 69, p. 371, 1996.

[12] G.E. Jellison, Jr. and F.A. Modine, "Parameterization of the optical functions of amorphous materials in the interband region (erratum)," *Applied Physics Letters*, vol. 69, p. 2137, 1996.

[13] H. Nozaki, M. Onoda, M. Sekita, K. Kosuda, and T. Wada, "Variation of lattice dimensions in epitaxial SnS films on MgO(001)," *Journal of Solid State Chemistry*, vol. 178, pp. 245-252, 2005.